Engineering Fracture Mechanics 77 (2010) 437–451

Contents lists available at ScienceDirect

Engineering Fracture Mechanics

journal homepage: www.elsevier.com/locate/engfracmech

On the sharpness of straight edge blades in cutting soft solids: Part II – Analysis of blade geometry

C.T. McCarthy [a,*], A. Ní Annaidh [b], M.D. Gilchrist [b]

[a] Materials and Surface Science Institute (MSSI) and the Department of Mechanical and Aeronautical Engineering, University of Limerick, Limerick, Ireland
[b] School of Electrical, Electronic and Mechanical Engineering, University College Dublin, Dublin 4, Ireland

ARTICLE INFO

Article history:
Received 8 December 2008
Received in revised form 14 October 2009
Accepted 21 October 2009
Available online 30 October 2009

Keywords:
Sharpness
Cutting
Elastomers
Finite element analysis
Indentation

ABSTRACT

In Part I of this paper a new metric, titled the "blade sharpness index" or "BSI", for quantifying the sharpness of a straight edge blade when cutting soft solids was derived from first principles and verified experimentally by carrying out indentation type cutting tests with different blade types cutting different target or substrate materials. In this Part II companion paper, a finite element model is constructed to examine the effect of different blade variables including tip radius, wedge angle and blade profile on the BSI developed in Part I. The finite element model is constructed using ABAQUS implicit and experiments are performed to characterise the non-linear material behaviour observed in the elastomeric substrate. The model is validated against the experiments performed in Part I and a suitable failure criterion is determined by carrying out experiments on blades with different tip radii. The paper finds that a simple maximum stress criterion is a good indicator for predicting the onset of cutting. The validated model is then used to examine blade geometry. It is shown that finite element analysis is an important tool in helping to understand the mechanics of indentation. Furthermore, the study finds that all the blade geometric variables have an influence on the sharpness of a blade, with the BSI being most sensitive to tip radius. Increasing the tip radius and wedge angle decreases the sharpness of the blade.

1. Introduction

The *sharpness* of a cutting instrument is a critical parameter in all cutting applications because it directly influences the forces generated during cutting, the mechanics of cutting, the service life of the cutting edge, and the surface finish or roughness of the cut surface. In Part I of this companion paper [1] a quantitative metric for the sharpness of a straight edged blade was developed and critically assessed for different blade types and target or substrate materials (i.e. the material being cut). The dimensionless metric, referred to as "the blade sharpness index" or "BSI" is relevant to a wide range of applications associated with cutting soft solids, including the meat and food processing industries, surgery, forensic medicine, zoology, and some machining processes. The generalised form of the BSI is given as:

$$\mathrm{BSI} = \frac{\int_{\delta_i} F dy}{\delta_i t J_{Ic}} \tag{1}$$

where F is the cutting force, dy is an increment of blade displacement in the loading direction, δ_i is the blade displacement or indentation depth at which a cut first initiates in the substrate material, t is the substrate thickness and J_{Ic} is the Mode I

* Corresponding author. Tel.: +353 61 234334; fax: +353 61 202944.
E-mail address: conor.mccarthy@ul.ie (C.T. McCarthy).

0013-7944/$ - see front matter © 2009 Elsevier Ltd. All rights reserved.
doi:10.1016/j.engfracmech.2009.10.003

Nomenclature

dy	increment of blade displacement
A	cross-sectional area
E	energy
F	applied force
W	strain energy density
h	length of cut surface
J_{Ic}	Mode I fracture toughness
t	thickness of substrate material
α_i	Ogden constant
δ_i	depth of blade indentation (to initiate a fracture)
ε	direct engineering strain
λ	stretch ratio
μ_i	Ogden constant
σ	direct stress
τ	shear stress

fracture toughness of the substrate. This index relates the energy required to initiate a cut in a substrate (the numerator in Eq. (1)) to the fracture toughness and thickness of the particular substrate and to the indentation depth required to penetrate the substrate. The particular mechanism of cutting for which this metric has been developed is termed "indentation cutting" in which a blade is pushed perpendicularly through a substrate akin to creating a Mode I fracture surface. The indentation type cutting is representative of guillotining, chopping, and certain carving processes. In Part I [1], it was shown that for an infinitely sharp blade the BSI would tend towards zero, whilst increasing values of BSI would represent increasing levels of blade bluntness. The index has been verified for a range of blade sharpness conditions and for a range of soft elastomeric substrates under different rates of loading.

A significant volume of literature exists on testing and modelling the indentation and cutting processes [1–23]. In general, indentation studies have only been interested in the response of the indenter and substrate before cutting initiates [1–9], while cutting studies [10–23] have generally examined the long term response of the cutting process, where material separation or cutting reaches a steady state.

For the indentation studies examined, researchers have used experimental [2–5] and numerical [4–7] methods, such as finite element analysis [4,6] and/or theoretical models [2,3,5], to predict the response of the indenter and substrate. The substrates examined have ranged from very hard materials, such as ceramics [6] and steels [7], to very soft materials such as elastomers and skin [2–5,8,9,21,22]. Studies examining elastomeric substrates have, in general, modelled them using strain energy density functions, such as the Mooney [2], Ogden [4], Yeoh [4] or neo-Hookean [5,9] models. In order to apply Hertzian contact theory to model the indentation process, one study [8] modelled the elastomeric substrate as linear elastic with a very low Young's modulus and a Poisson's ratio close to 0.5. A characteristic common to a number of indentation studies is the *J*-shaped load–deflection curve observed as the level of indentation increases [2,3,8,22]. This non-linearity is due to the increase in the contact area between the indenter and the substrate as the indentation progresses. Some studies have examined friction between the indenter and the substrate [4,7,8] while others have ignored it [5,6]. A major difficulty with modelling friction is experimentally determining the friction coefficient at the contact interface.

In most of the cutting papers reviewed [10–17,19] the work piece or substrate material was modelled with deformable finite elements and most studies used a two-dimensional finite element formulation [10–13,15,16,19]. Where anisotropy existed in the substrate, a full three-dimensional analysis was employed [14]. On the other hand, the cutting tool or instrument has been modelled as both rigid [10,11,15,16] and/or deformable [12,16–20]. In the deformable cases, the authors were interested in determining temperature distributions [12,18], wear [16,19], displacements [17], or Mode shapes [20] in the cutting tool. Most of these studies have considered a contact and friction analysis between the cutting tool and the substrate. However, very little information was given on the actual value of the coefficients of static and dynamic friction at the tool/substrate interface, with most researchers just estimating it. Many different approaches such as cohesive zone models [10], the Cockroft–Latham model [11], virtual crack extension method [14], fracture mechanics [14] and element deletion using a shear failure criterion [16] have been used to simulate material separation as the cutting commences. To solve the problem many different commercially available finite element codes, such as ABAQUS [10,16], DEFORM-2D [11,19], MARC [12,13,15], SAMCEF [14] and ANSYS [17,18] have been used, with no fundamental underpinning reason for the particular choice of code.

As can be seen, extensive research has been carried out on both the indentation and cutting processes and the above survey is just a sample of the many papers available on the subjects. However, none of the studies reviewed have been concerned with modelling with the specific goal of determining the sharpness of the indenter or cutting instrument. The Part I companion to this paper described physical experiments to determine the sharpness of straight edged blades and a quantitative metric was derived (Eq. (1)). In this Part II paper, a finite element study is carried out to examine the effect of blade geometry on the sharpness index that was derived and verified in Part I. The geometric variables that are examined include

blade tip radius, blade tip angle and blade type (i.e. both single wedge angle and double wedge angle blades are examined). The approach taken here is to first build and validate a finite element (FE) model of a Swann-Morton blade cutting a polyurethane substrate (for which extensive experimental results are available from Part I) and then, secondly to use this validated model to systematically examine the geometric variables listed above.

2. Problem description

In the companion Part I paper [1], indentation type cutting experiments were performed where straight edged blades were pushed through elastomeric substrate materials as illustrated in Fig. 1a. The blade was forced into the substrate material under a constant velocity and the reaction load on the blade (i.e. F) was measured. The substrate material deformed to a

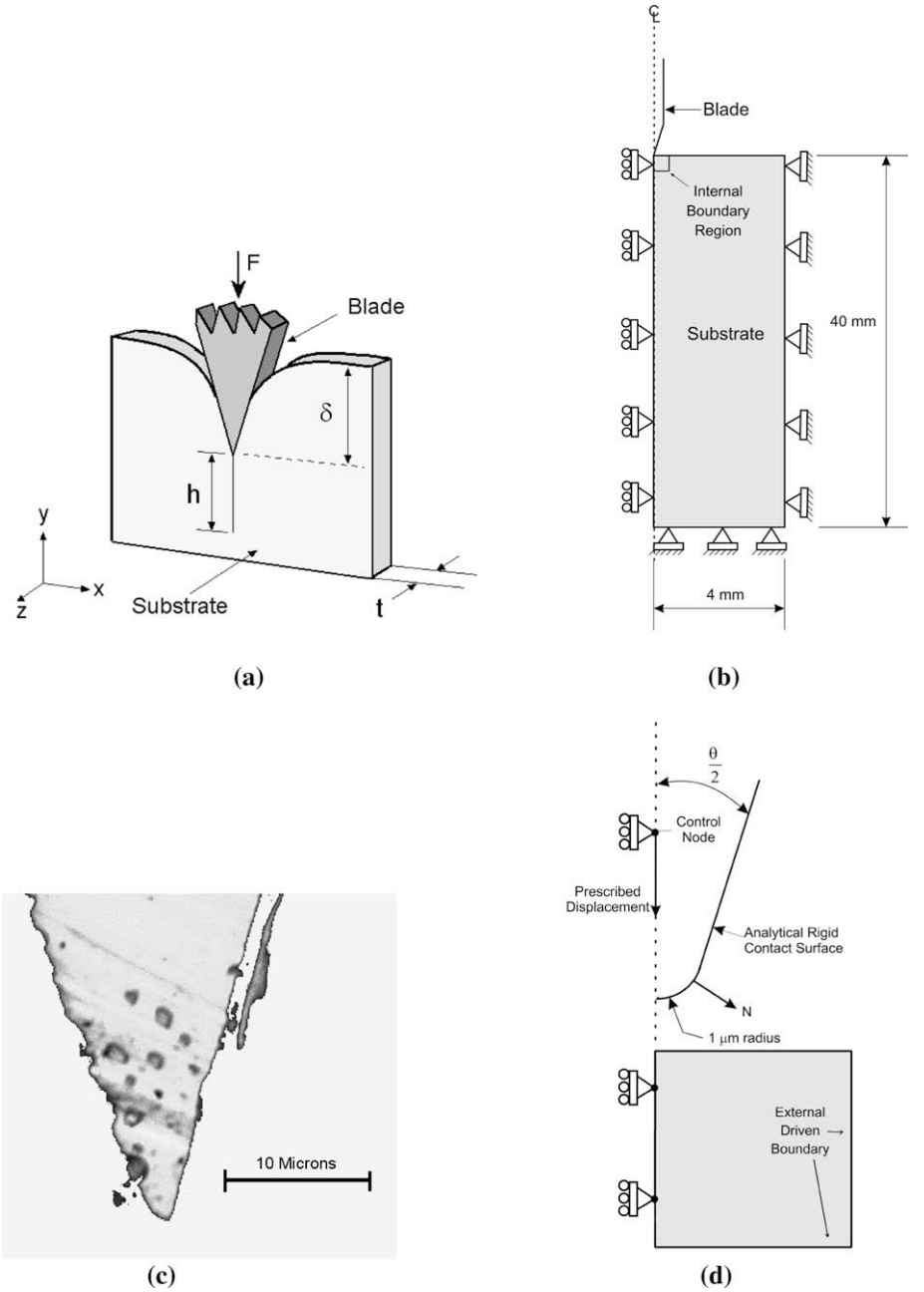

Fig. 1. (a) Idealisation of cutting process, (b) corresponding finite element model showing boundary conditions, (c) micrograph of actual blade tip, (d) close-up of blade tip contact body and boundary conditions on control node (note: pictures not to scale).

penetration depth δ_i and at this point fracture or a cut initiated in the substrate. Upon further loading, the substrate material separated and cutting commenced. It was found by carrying out indentation experiments with lubricated and non-lubricated blades that δ_i was not sensitive to friction at the interface and so friction is not considered in this analysis. The length of the cut surface was denoted by h and the thickness of the substrate by t. The experiments were performed with the main aim of deriving and validating a new metric to quantify blade sharpness (Eq. (1)) and the reader is referred to Part I [1] for a detailed description of both the experiments and the BSI derivation.

In this Part II paper, a finite element model of the cutting experiments carried out in Part I is developed in the ABAQUS [24] non-linear finite element code. Since the loads were applied quasi-statically the implicit version of ABAQUS was used. The main focus of the model is to capture the indentation process since this is sufficient to calculate the BSI (Eq. (1)). The finite element model is based on the experiments of a Swann-Morton No. 16 straight edged blade indenting the polyurethane substrate (Hardness: 40 Shore A) performed in Part I. This blade and substrate will subsequently be referred to as the SM blade and PU substrate, respectively. Also, in Part I a second type of blade of razor configuration (manufactured by CAMB Machine Knives International (type CMK 152)) was examined. This blade had a double wedge angle, thus providing an interesting alternative profile and so is examined here and will subsequently be referred to as the CAMB blade.

The paper is structured as follows: Firstly, a finite element model is constructed in ABAQUS implicit and then validated against experiments performed in Part I. The validated model is used to examine the stress state under the blade tip and then used in conjunction with PU strength data to derive a suitable criterion for predicting the onset of fracture or cut formation in the substrate. The failure criterion is then verified by comparing the model to experiments performed on blades with different blade tip radii. Having established the failure criterion, a parametric study is then carried out to examine the effect of blade tip radius, wedge angle and blade type (i.e. both the SM single-tip and CAMB double-tip blades are modelled) on the BSI index given by Eq. (1).

3. Finite element model

3.1. Geometry and boundary conditions

The geometry used to model the experimental cutting trials is shown in Fig. 1b. Due to mirror symmetry only one half of the blade and substrate were modelled. To simulate the support plate and anti-buckle guides of the testing apparatus, two sides of the plate were fixed (i.e. displacements $u = v = 0$). A symmetry boundary condition was applied to the left edge of the substrate. The remaining top side of the substrate was not constrained.

The blade geometry was obtained from micrographs taken from sections of the SM blade, as shown in Fig. 1c. As can be seen, the blade tip is approximately round of 1 μm approximate radius and so was modelled using a semi-circular contact body. The blade tip angle was also measured directly from the micrographs.

As the blade was constructed from steel, which is over three orders of magnitude stiffer than the PU substrate, it was considered rigid with respect to the substrate and hence modelled using an analytical rigid contact body, as shown in Fig. 1d. The motion of the blade was specified via a contact control node where boundary conditions were applied to suppress rotations in the xy-plane and displacements in the x-direction, thus constraining the blade to move only in the negative y-direction (as in the experiment). A finite (which depended on the model under consideration) downward y-displacement was applied to the control node to indent the blade into the substrate. An automatic time stepping algorithm was used to overcome inherent convergence problems due to the non-linear behaviour associated with large-deformation, non-linear material behaviour and contact occurring simultaneously.

3.2. Finite element mesh and sub-modelling approach

A very fine mesh is needed to capture the near singular stress state under the blade tip. However, a major drawback with this problem is that the blade tip is of the order of 1 μm while the substrate's dimensions are four orders of magnitude greater. Standard meshing approaches such as modelling the entire substrate with elements having characteristic dimensions of the order of 1 μm or less or using many levels of mesh transitioning are computationally inefficient, with the latter approach also leading to elements with very poor aspect ratios in some regions. Hence, to overcome these shortfalls, a sub-modelling procedure was employed.

With the sub-modelling procedure the full or global model is first run using a reasonably coarse mesh. An internal boundary region is defined (as highlighted in Fig. 1b) and this *internal* boundary region then becomes the *external* boundary region for the sub-model, as shown in Fig. 1d. The deformed shapes of these regions are shown in Fig. 4c. The nodal displacements on the boundary region in the global model are stored in an output file for each time increment and then used to drive the boundary of the sub-model. Hence, in the sub-model it is only necessary to model a small portion of the substrate, since the influence of the removed portion is represented through the driven boundary condition. This facilitates introducing a very fine mesh in the sub-model and thus allows the stresses and strains under the 1 μm blade tip to be captured efficiently. The characteristic length for the elements under the blade tip was 0.1 μm. To ensure consistency between the global model and sub-model, a check was carried out to ensure that the load–displacement curves from both models matched. Finally, due to

the relatively small thickness of the substrate (2.25 mm) a state of plane stress was assumed and hence fully integrated plane stress elements (CPS4) were used.

3.3. Material model

3.3.1. Experimental characterisation of the PU substrate material

Tensile tests were performed to determine the form of the constitutive response for the substrate material. This characterisation was carried out in accordance with a British Standard for the physical testing of rubber [25]. This standard governs a considerable number of testing parameters such as specimen shape, loading rate and calculation of results.

Following this standard, dumb-bell specimens were cut (using a die cutter) from the same sheet of material used for the indentation experiments performed in the Part I paper [1]. In the experiment, the specimen strain was measured using a non-contact laser extensometer and so it was necessary to tab each sample with 3 M reflective tape at a fixed gauge length of 25 mm (in accordance with the standard). Fig. 2a shows the experimental set-up. The specimens were mounted in a Tinius-Olsen universal testing machine and loaded in tension at a rate of 500 mm/min (in accordance with the standard). The dumb-bell specimens were held tightly between two grips, one fixed to the frame of the testing machine and the other attached to the moving crosshead via a load-cell. Coarse sandpaper was inserted between the grips and the specimens to prevent slipping at high elongations. The laser extensometer was fixed to the frame of the testing machine via a connecting support arm. The laser housing did not move during the test. However, the laser beam did move in order to track the positions of the reflective tabs for subsequent measurement of the specimen strain. A close-up image of the specimen at the start of the test is shown in Fig. 2b. The laser beam scans along the specimen and its image can be clearly seen along the centre line of the specimen in Fig. 2b.

The constitutive response from a typical test is shown in Fig. 3. The true or Cauchy stress, σ_{true}, was determined from the following equation:

$$\sigma_{\text{true}} = \lambda \frac{F_{lc}}{A_0} \tag{2}$$

where F_{lc} is the force obtained from the load-cell, A_0 is the original cross-sectional area within the gauge length of the specimen and λ is the stretch ratio in the loading direction and was obtained from the following equation:

$$\lambda = 1 + \varepsilon_{LE} \tag{3}$$

where ε_{LE} is the strain in the loading direction as determined from the laser extensometer. From Eq. (3) it can be clearly seen that at zero strain, the stretch ratio is exactly 1: hence the offset on the stretch ratio axis in Fig. 3. The curve in Fig. 3 shows the classical rubber response with a pronounced upturn in the stress at high elongation (i.e. high λ). This pronounced upturn produced some variability in measured strengths from the six repeats of the test, as listed in Table 1. The specimens failed at an average true stress of 114.31 MPa with standard deviation (SD) of 11.29 or 9.8%. The average specimen stretch ratio at

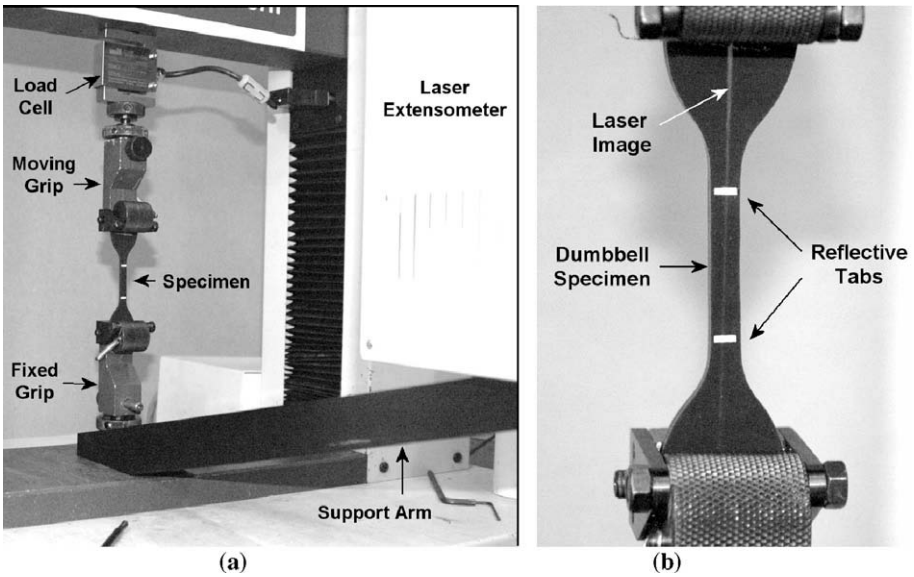

Fig. 2. Experiment to characterise the substrate material (a) experimental set-up with the laser extensometer, (b) close-up of the test specimen before testing showing laser image and reflective tabs.

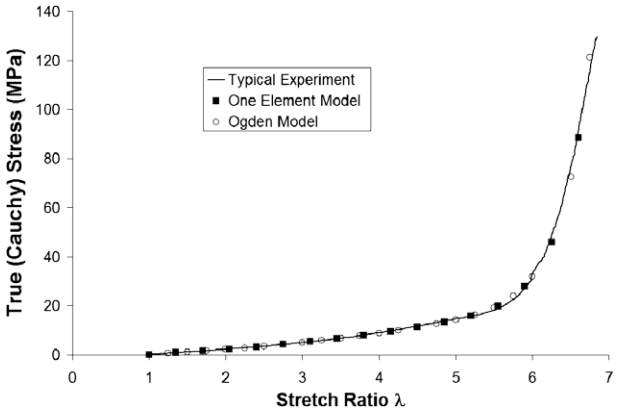

Fig. 3. True stress vs stretch ratio for the uni-axial tensile test on the elastomeric substrate. Figure also shows the Ogden model fit and the single element test result.

Table 1
Strength data for the PU material.

Test no.	σ_{UTS} (MPa)	σ_{UTS} (Ave/SD)	λ_{max}	λ_{max} (Ave/SD)
1	123.76	114.31/11.29	6.59	6.62/0.13
2	102.78		6.55	
3	112.11		6.52	
4	101.31		6.51	
5	129.72		6.84	
6	116.27		6.71	

failure was 6.62 with an SD of 0.13 or 1.9%. This means the specimens elongated to 6.62 times their original length before rupture. This material strength data is used later to help predict the onset of cut formation in the finite element models.

3.3.2. Hyperelastic material model

As discussed in Section 1, many researchers modelling indentation of elastomeric materials have used different strain energy density functions [2,4,5,9] to capture the non-linear constitutive behaviour observed in their experiments. Another reason for this is that elastomers are generally considered incompressible, meaning that they have a Poisson's ratio equal to or very close to 0.5 and so standard material models are ineffective. Hence, in order to model the non-linear material behaviour of the PU substrate, a number of strain energy density functions were examined. It was found that a three term Ogden [26] strain energy density function with the coefficients listed in Table 2 gave the best fit to the experimental data as it effectively captured the pronounced upturn in the stress–strain curve, as shown in Fig. 3. It should be noted that the value for μ_2 is very small and could be considered as zero. However, it was found that setting it to zero resulted in the Ogden model not capturing the sharp upturn in the stress at high elongations. Lower order Ogden functions were also found not to sufficiently capture this sharp upturn in stress. Finally, a one-element test was carried out to ensure that the material model reproduced the constitutive response, and this is also shown in Fig. 3.

3.4. Interface model

The final important aspect of the model is to ensure that the surface interaction between the blade and substrate is correctly represented. Large displacements were expected in both the blade and the substrate and so a finite sliding contact algorithm, which allows for arbitrary separation, sliding and rotation between surfaces, was implemented.

Table 2
Experimentally determined Ogden material parameters.

Coefficient	$i = 1$	$i = 2$	$i = 3$
μ_i	0.29	1.2e−16	0.42
α_i	2.33	23.18	−1.59

3.5. FE model validation

The deformed shape and load–deflection characteristics were used to validate the proposed model. For validation purposes, an indentation experiment was carried out using a lubricated SM blade and PU substrate and so the interface was assumed frictionless in the model. The blade indentation displacement chosen for the comparison was 2 mm: this represented the indentation level just where a cut initiated in the substrate, as described in detail in the Part I paper [1].

A visual comparison between the actual and predicted deformed shape is shown in Fig. 4a. As can be seen, the deformation characteristics in the model are very similar to those of the experiment, with high local deformation being observed under the blade tip. To provide a more quantitative comparison, the vertical displacement of the top edge in the experiment and model are plotted in Fig. 4b. As can be seen, good agreement was obtained, thus providing confidence in the model.

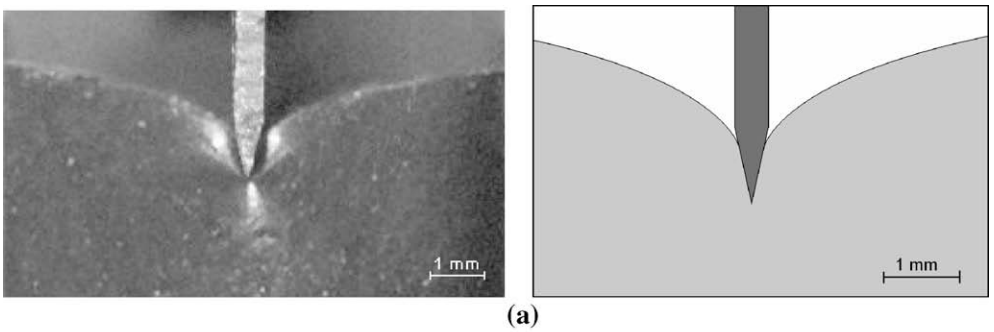

(a)

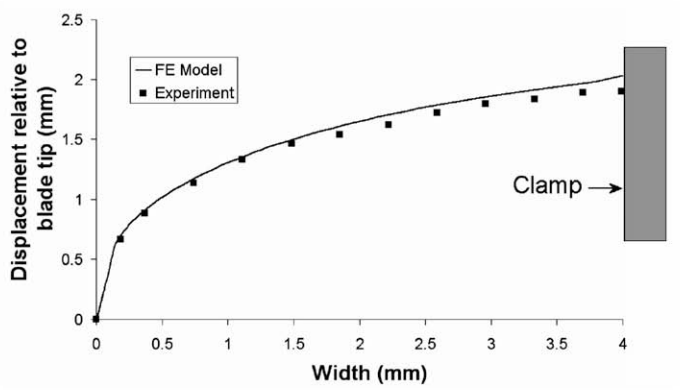

(b)

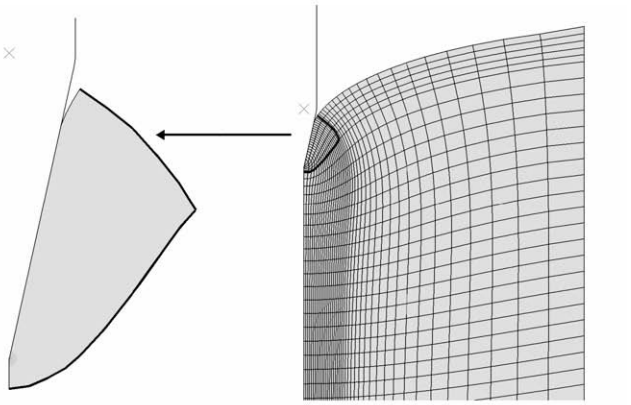

(c)

Fig. 4. (a) Experimental and numerical deformed shape at a blade displacement of 2 mm (note: pictures to similar but not exact same scale), (b) vertical displacement of the free edge (i.e. top edge) in the experiment and model, (c) local sub-model (FE mesh removed for clarity) and global model.

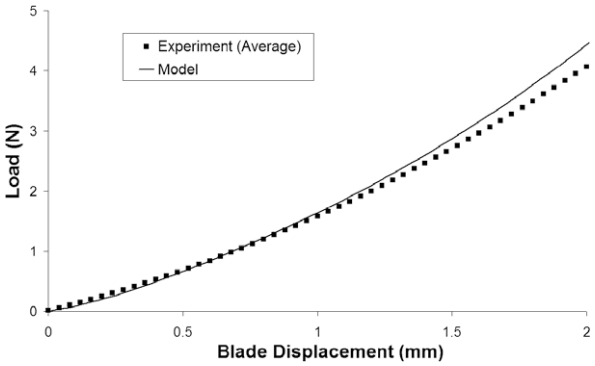

Fig. 5. Load–displacement response for the experiment and model.

Fig. 4c shows the deformed shape of the local sub-model and global finite element model. The deformed *driving* and *driven* boundaries used in the sub-modelling technique (highlighted in the picture) have undergone extensive deformation as a result of the highly localised loading from the blade. As can be seen, the sub-model is only a small portion of the global model, which facilitated the use of a very fine mesh (not shown for clarity). Extensive deformation is observed under the blade tip which leads to large stress gradients at that location, as depicted in the stress plots in Fig. 6.

Next, the load–deflection behaviour was examined. The load acting on the blade was taken from the control node in the model while it was measured by the load-cell in the experiment. The corresponding load–displacement curves are shown in Fig. 5, where it can be seen that the model provides a realistic prediction of the load–deflection behaviour. Both the experiment and model display a *J*-shaped load–deflection response, which is a characteristic of indenting soft materials [2,3,8,15,21,22,27]. However, the experiment is slightly less stiff than the model, which is most likely due to some slipping of the substrate in the grips (note: the model assumed a perfectly clamped boundary, see Fig. 1b).

The final stage of the validation process was to carry out a convergence study to ensure the solution was mesh independent. The approach taken was to increase the mesh density in the sub-model only, since this model was used to capture the high stress and strain gradients under the blade tip. The criterion used for the mesh comparison was the maximum principal strain. Three different mesh densities were examined, namely a reasonably course mesh with 3876 degrees of freedom (DOF) yielding a strain value of 6.56, a medium mesh with 5151 DOF yielding a strain value of 6.45, and a very fine mesh with 10251 DOF yielding a strain value of 6.39. As very little change was seen in the maximum principal strain between the three models, this indicated that the model was mesh independent. The medium density mesh was used for all subsequent modelling. In summary, the proposed model was considered to have been validated and sufficiently accurate to proceed to examine the effect of blade geometry on the BSI.

4. Results

Before examining the effects of blade geometry on the BSI, the model is first examined to investigate its deformation and stress characteristics, with the overall aim of deriving a suitable failure criterion for predicting the onset of cutting. For the SM blade cutting a PU substrate, it was found that a cut first initiated at a blade indentation depth of 2 mm. Hence, this indentation depth is used to examine the stress state in the substrate at the onset of cut formation.

4.1. Stress analysis

Before proceeding, it should be noted that the models were analysed as half models and so the full model stress plots in Fig. 6 were generated using a post-processing mirroring technique. The stress in the *x*-direction, σ_{xx}, is shown in Fig. 6a. This stress is transverse to the loading *y*-direction and would tend to pull the substrate apart, leading to a Mode I type fracture when the cut initiates. As can be seen in the Figure the stress σ_{xx} actually peaks slightly ahead of the blade tip (approximately 0.2 μm) and so the cutting would most likely initiate there. However, with increased loading, the cut would propagate very quickly so that the crack tip would be adjacent to the blade tip. The stress in the loading *y*-direction, σ_{yy}, shown in Fig. 6b, can be seen to be highly compressive beneath the blade tip, as expected. This stress peaks directly under the blade tip and would cause the substrate to bulge out-of-plane. In the limit case, this stress would lead to local instabilities, such as buckling or wrinkling [28], as observed in the blunt blade experiments in the Part I paper [1]. The σ_{yy} stress has a peak tensile zone located at the side of the blade (exactly where the rounded tip and straight side of the cutting edge meet) and this could lead to tearing at that location. However, this stress is significantly lower in magnitude (41 MPa) than the σ_{xx} tensile stress region under the blade tip (approximately 100 MPa), shown in Fig. 6a. Hence, it is more likely that failure will initiate under the blade tip. For completeness of the plane stress analysis, the shear stress in the *xy*-plane, τ_{xy}, and the von-Mises stress $\sigma_{von\text{-}Mises}$ are plotted in Fig. 6c and d, respectively. The shear stress peaks at the blade tip at approximately 45° to the vertical

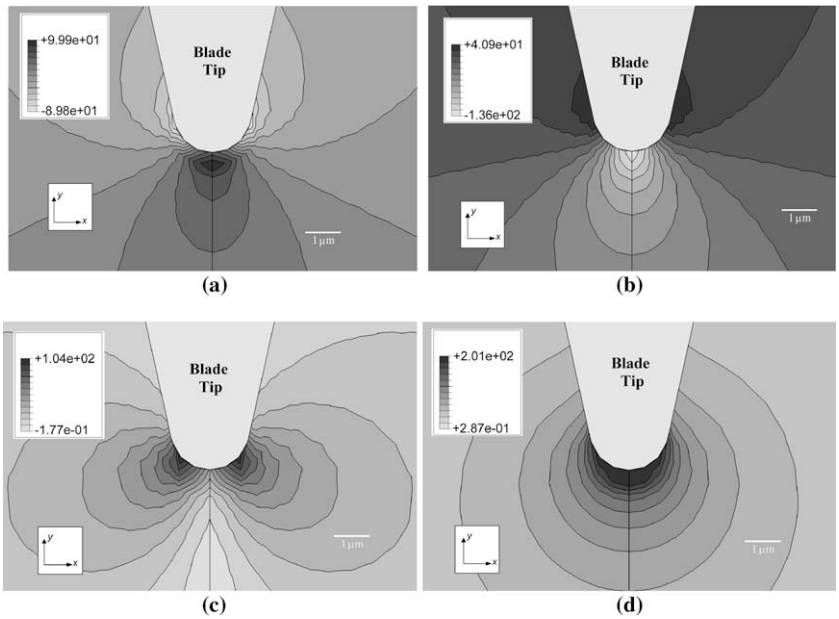

Fig. 6. Stress fields at the blade tip at 2 mm blade indentation (note: all units of stress are MPa) (a) σ_{xx}, (b) σ_{yy}, (c) τ_{xy} (d) $\sigma_{\text{von-Mises}}$.

and the von-Mises stress peaks directly under the blade tip and propagates outwards in a circular manner throughout the PU substrate.

4.2. Failure criterion

For quantitative purposes, the stresses are plotted as a function of the distance from the blade tip in Fig. 7. The co-ordinate system used for plotting these stresses is shown in the insert to Fig. 7. Also plotted in Fig. 7 are the maximum, minimum and average failure stresses, as determined from the experimental uni-axial tensile tests presented in Section 3.3.1. As can be seen, there is a very steep gradient for each stress immediately ahead of the blade tip, thus highlighting the near singular nature of this problem. It can also be seen that the predicted tensile stress under the blade tip σ_{xx} = 100 MPa is very close to the average tensile strength of the material, σ_{UTS} = 114 MPa, especially when the variability in the measured strengths is considered (Table 1). Previous work on the puncture characterisation of rubber membranes has shown that the puncture strength is lower than the tensile strength or biaxial strength of the material [2]. Hence, it was apparent that a simple maximum stress criterion given by,

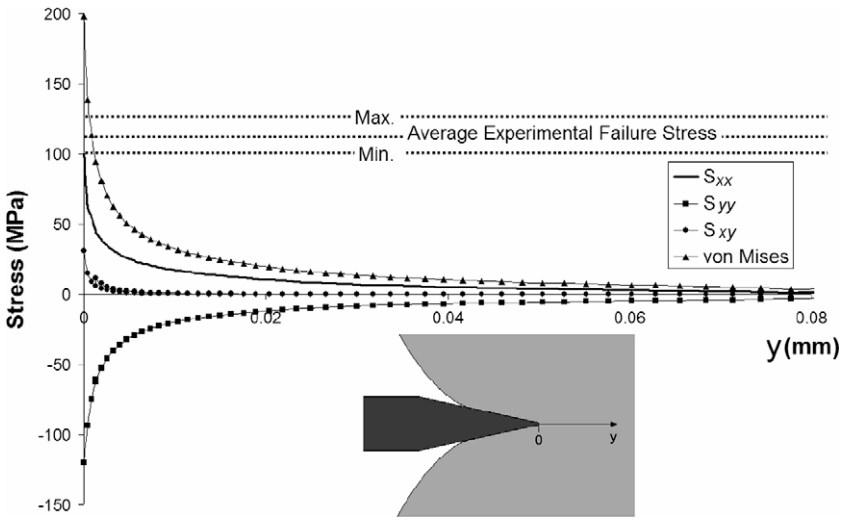

Fig. 7. Stress distributions ahead of the blade tip (insert shows the co-ordinate system used).

$$\frac{\sigma_{xx}}{\sigma_{\mathrm{UTS}}} = 1 \tag{4}$$

may be a good elastic predictor for predicting the onset of cut formation in the elastomeric substrate. Examination of the von-Mises stress in Fig. 7 indicates that it is approximately 200 MPa at the point of cut formation, which is significantly higher than the average material strength (114 MPa). Hence, the von-Mises stress does not, in this case, seem to be controlling failure and if used would lead to a very conservative estimate for onset of cut formation.

In order to examine if the σ_{xx} stress was controlling the onset of cut formation, a number of experiments were carried out in which virgin blades were artificially blunted in a specially designed blunting rig. This rig allowed the tip radius to be varied systematically from 1 μm (i.e. a virgin blade) up to 5 μm in a controlled and repeatable manner and will be reported on in a future publication. Fig. 8 shows some different blade tips after being blunted and as can be seen the tips are approximately round. Different blade tips, with radii ranging from 1 to 5 μm were tested and the resulting indentation depth to cut formation, δ_i, values were recorded. These results are shown along with model predictions in Fig. 8, and as can be seen good agreement was obtained, suggesting that the maximum stress criterion is a good measure for predicting the onset of cut formation. Therefore, this criterion is used as the failure measure for the different blade geometries examined in Section 4.3 below.

4.3. Effect of blade geometry on the BSI

As determined in the previous section, when the σ_{xx} stress in the substrate under the blade tip reaches the uni-axial tensile strength of the material, a cut is assumed to initiate in the substrate. The BSI can then be evaluated from the models by first determining the blade indentation depth required to achieve this failure stress in the substrate, thus determining δ_i. Then, from the load–deflection response, the energy needed to reach δ_i can be determined by integrating the load–displacement curve, i.e. computing the $\int_{\delta_i} F dy$ term in Eq. (1). The substrate thickness $t = 2.25$ mm and the fracture toughness was determined in Part I of the paper as $J_{Ic} = 3.67\mathrm{kJm}^{-2}$. The BSI can then be calculated directly from Eq. (1).

4.3.1. Effect of tip radius

To examine the effect of tip radius on the BSI, radii of 1–5 μm were examined. Radii greater than 5 μm were not considered as such blades were considered to be unrealistically blunt. The results of this study are plotted in Fig. 9, where it can be seen that the BSI increases in a mildly non-linear fashion with increasing tip radius. It should be noted that increasing values of BSI indicate increasing levels of blade bluntness.

Also plotted in Fig. 9 is the force needed to initiate a cut in the substrate. As can be seen, for a virgin blade (i.e. tip radius = 1 μm) the force required is approximately 4.5 N. The force increases approximately linearly with increasing tip radius and so it is apparent that the sharpness of the blade is quite sensitive to the tip radius. In physical terms, this means that it would be important to maintain tight control over the size of the tip radius during manufacture of the blade. In addition, to avoid blunting during cutting it would also be important to minimise any increase in the tip radius due to, for example, blade tip wear.

4.3.2. Effect of wedge angle

To examine the effect of wedge angle, all other geometric variables, such as tip radius, blade thickness and length were kept constant and equal to that of the SM blade. For this study, blade angles of 10–45° were examined and the resulting BSI

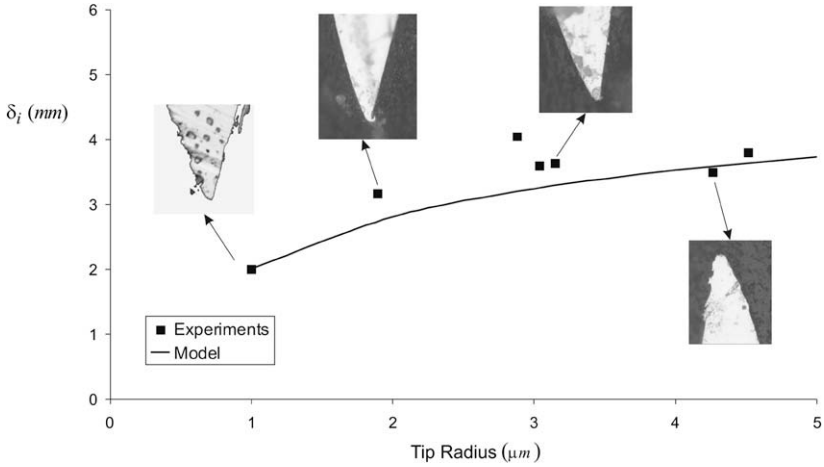

Fig. 8. Predicted and measured δ_i values as a function of blade tip radius.

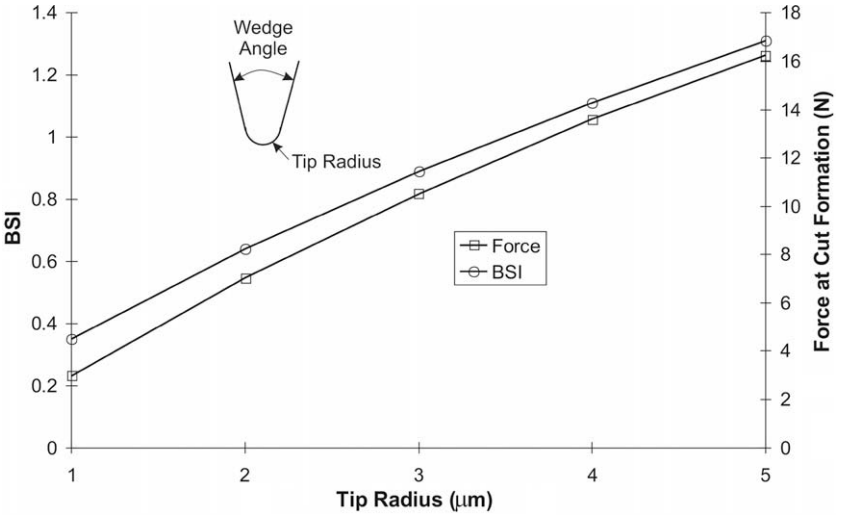

Fig. 9. Blade sharpness index (BSI) as a function of blade tip radius (wedge angle kept constant at 25°).

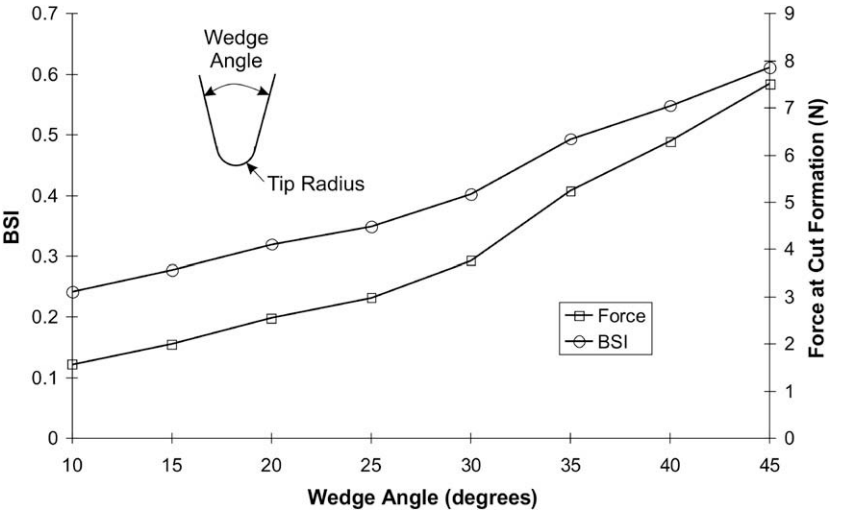

Fig. 10. Blade sharpness index (BSI) as a function of blade wedge angle (tip radius kept constant at 1 μm).

values are plotted in Fig. 10. As can be seen, the BSI distribution is approximately a bilinear function of blade angle with a change in slope observed around 25°. The lower slope region indicates that the BSI is initially less sensitive to variations in wedge angle. For example, by reducing the wedge angle from 25° to 20° degrees the BSI changes from approximately 0.23 to 0.20, indicating a small improvement in blade sharpness. While this might be considered desirable, reducing the wedge angle by 5° considerably reduces the amount of material at the tip available to resist the compressive forces acting at the tip, thus reducing the tip's stability, i.e. the blade would be more likely to bend or buckle.

The force at cut formation is also plotted as a function of wedge angle in Fig. 10. As can be seen the force increases due to increases in wedge angle, but the relative increase is significantly lower than that observed for the variation in tip radius (shown in Fig. 9.) Hence, it is apparent that tip radius is a more important parameter with respect to the sharpness of the blade.

4.3.3. Effect of blade profile

Cross-sections of the CAMB and SM blades are shown in Fig. 11a and b, respectively. Thus far, all finite element modelling of blade geometry has been focused on the single wedge angle profile of the SM blade (25° wedge angle). However, in order to examine the effect of a double wedge angle, a model based on the CAMB blade cross-sectional profile was developed. An identical model to that used for the SM blade was constructed, with the exception of the blade geometry being different. A contour plot of the stress in the x-direction, σ_{xx}, for this double wedge angle profile is shown in Fig. 11a along with the

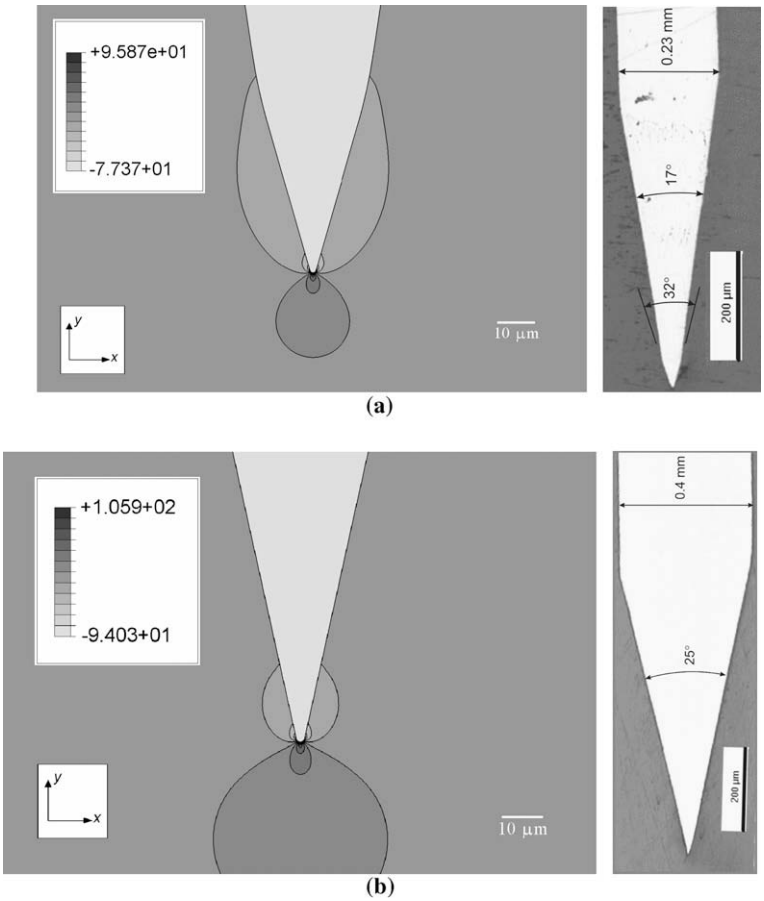

Fig. 11. Stress in the *x*-direction, σ_{xx}, at 2 mm blade indentation (a) CAMB blade (maximum tensile stress = 95.87 MPa), (b) SM blade (maximum tensile stress = 105.9 MPa).

corresponding stress distribution of the single wedge angle blade in Fig. 11b. For comparison, both plots are shown at the same blade indentation depth (approximately 2 mm). As can be seen, both blades produce similar stress patterns in the substrate material. However, the maximum stress is approximately 10% higher in the single wedge angle profile, indicating that it is a sharper blade. The reason for this is that the wedge angle closest to the tip for the double wedge angle CAMB blade is 32°, as shown in the blade cross-section in Fig. 11a, whereas it is a constant 25° for the single wedge angle SM blade, as shown in Fig. 11b. Hence, it is apparent that the wedge angle closest to the tip determines the sharpness of the tip, as would

Table 3
Summary of experimentally and numerically derived BSI values.

Blade type[a]	Tip radius, μm	Tip blade angle, °	Secondary blade angle, °	Experimentally determined BSI	Numerically determined BSI
SA	1	10	–	–	0.122
SA	1	15	–	–	0.156
SA	1	20	–	–	0.198
SA	1	25	–	0.216 ± 0.02[b]	0.232
SA	2	25	–	0.61 ± 0.11	0.546
SA	3	25	–	0.77 ± 0.04	0.818
SA	4	25	–	–	1.058
SA	5	25	–	–	1.263
SA	1	30	–	–	0.293
SA	1	35	–	–	0.408
SA	1	40	–	–	0.490
SA	1	45	–	–	0.584
DA	1	32	17	0.251 ± 0.01[b]	0.267

[a] SA = single angle, DA = double angle.
[b] Determined in the Part I paper [1].

be expected. The BSI for the double wedge angle was computed as 0.267 which is higher than that of the single wedge angle blade with a BSI of 0.232. These trends are in good agreement with the experimentally determined BSI values (from Part I), as shown in Table 3.

5. Summary

All of the BSI values that were determined numerically and experimentally are listed in Table 3. Some of the experimental values were derived in the companion Part I paper [1]. As can be seen, there is good agreement between the numerical and experimental values for the two cases considered, especially when experimental measurement error is taken into consideration.

6. Discussion

In a companion Part I paper [1] a new metric for quantifying the sharpness of a straight edged blade when cutting soft solids was derived from first principles and experimentally verified by carrying out indentation type cutting tests using different types of blades to cut different target or substrate materials. It was found that this blade sharpness index or BSI was independent of the substrate material being cut and the cutting rate and so it was concluded that it pertained to the blade only. Lower values of BSI corresponded to sharper (i.e. less blunt) blades. The experiments revealed that a sharp blade (i.e. a virgin surgical scalpel blade) had a BSI of approximately 0.2 while a blunt blade (i.e. an artificially blunted blade was used) had a BSI of approximately 0.5. These values gave an indication of the upper and lower bounds for both sharp and blunt BSI values, respectively.

This Part II paper has set out to numerically examine the effect of different blade geometric parameters, such as tip radius, wedge angle and blade type on the BSI. It was found that all these variables have an influence on the sharpness of a blade with the BSI being most sensitive to tip radius. While this finding might be the expected conclusion from the outset, this paper has quantified its importance, and has clearly shown that tip radius is a significantly more important parameter than wedge angle in sharpness measurement, which is not immediately obvious. Thus, based on these findings, it is apparent that the tip radius is the most important parameter in determining the sharpness of a blade, which is in agreement with the experimental work of Knight and others [29–32]. The BSI was found to be less sensitive to wedge angle. Increases in wedge angle resulted in increasing BSI values with its sensitivity increasing beyond 25°. Hence, it would appear that this angle is a good compromise between sharpness and stability of the tip.

The finite element model to determine blade sharpness took considerable effort to construct due to the highly non-linear nature of the problem. The non-linearities resulted from the substrate material being highly elastic and incompressible, thus requiring a strain energy density function to be employed. A geometrically non-linear analysis was also required to handle the large changes in geometry due to the highly localised deformation under the blade tip. The application of contact also led to the application of non-linear boundary conditions. A sub-modelling technique was invoked to help solve the problem efficiently. While this technique took time to debug, once the model was built and validated it was possible to carry out parametric studies very quickly. Thus, finite element analysis can contribute significantly to understanding the science of indentation.

It is known that sharp blades deform quite considerably during cutting, both elastically and plastically, and this can cause them to become worn and damaged after relatively short usage times, even when cutting soft materials. In this work, it was assumed that the blade was perfectly rigid, and while this is reasonably valid, it is recommended that the blade be modelled using deformable finite elements in any future investigations.

It has been found in this present work that a simple maximum stress theory could predict the onset of cut formation during indention well and certainly adequately for comparative purposes. The experiments performed with blades of varying tip radii verified the use of such a failure criterion and these experiments will be reported on in a future publication. It should be pointed out that the blade indentation depth to achieve the failure stress (i.e. δ_i) is used in the calculation of the BSI, not the failure stress itself. Hence, the maximum stress is only used to predict when the cut will initiate, while the BSI uses force and displacement (i.e. energy) data, which relates closely to the fracture toughness J. Furthermore, the failure criterion and the modelling approaches used in this work ignored viscoelastic and friction effects. It is expected that the viscoelasticity of the material would act to change the maximum stress considerably, making the result strain-rate dependant. Also, changes in the tip radius would change the local strain rate, even when the global loading rate is the same. Using a Prony series, it is relativity straightforward to implement viscoelasticity, but experiments are needed to calibrate the material parameters. It is thus recommended that viscoelasticity be included in future implementations of this model. Very little information is available on the coefficient of friction between surgical blades in contact with elastomeric materials for indentation type cutting scenarios. In Part I of this paper, it was found experimentally that friction did not have a significant influence on the BSI index and so friction was not considered in this analysis.

Finally, it should be noted that this study did not model the actual cutting process. To do this, a method to separate elements in front of the blade tip is needed. As discussed in Section 1, many authors used different approaches to achieve this and there is, as yet, no standard approach. Once cutting commences more advanced theories of fracture are required, since the tip of the cut forms a numerical singularity and stress based criteria are inappropriate. Some authors avoid this problem

by using cohesive zone models. However, these models require that the failure path be specified *a priori*, which calls into question the predictability of the model. Element deletion is another approach that has been used but such an approach requires a stress or strain failure criterion and so would be sensitive to the singularity at the crack tip. An interesting future development would be to model the cutting process using a multi-scale modelling strategy. With this approach the cut formation in front of the blade tip could be modelled at the micro- or even the nano-scale using discrete methods such as discrete element modelling, meshless methods or molecular dynamics. These could then be integrated into a global model of the bulk material, modelled at the continuum scale using a finite element approach similar to that used in this study.

7. Conclusions

This paper has set out to examine the effects of blade geometry on the sharpness of straight edged blades when cutting soft solids. A finite element model was constructed to simulate the indentation experiments carried out in the companion Part I paper [1]. This model considered contact at the blade/substrate interface and non-linear material behaviour. The model was experimentally validated and then used to examine the effect of blade tip radius, wedge angle and blade profile. These findings indicate that:

- A simple maximum stress criterion is a good indicator for predicting the onset of cutting.
- Blade sharpness increases with reducing tip radius.
- As the wedge angle reduces the blade sharpness increases. However, reducing the wedge angle would result in less material being present at the tip to resist the high compressive force acting there. This could lead to stability problems if the wedge angle is too small.
- Of the variables studied, blade sharpness was found to be most sensitive to the tip radius.
- Both single and double wedge angle blade tips were examined. It was found that the single wedge angle blade was sharper and this was due to the wedge angle nearest the tip being smaller than that of the double wedge angle blade. In conclusion, the wedge angle nearest the blade tip controls the sharpness of the blade, as would be expected.

Acknowledgements

The authors acknowledge Enterprise Ireland for funding this research under the auspices of the Commercialisation Fund (ATRP/2002/422B). Part of this publication has also emanated from research conducted with the financial support of Science Foundation Ireland (SFI) and the Irish Research Council for Science, Engineering & Technology (IRCSET).

References

[1] McCarthy CT, Hussey M, Gilchrist MD. On the sharpness of straight edge blades in cutting soft solids: part I – indentation experiments. Engng Fract Mech 2007;74(14):2205–24.
[2] Nguyen CT, Vu-Khanh T, Lara J. Puncture characterization of rubber membranes. Theor Appl Fract Mech 2004;42(1):25–33.
[3] Kohl JG, Bolstes RN. A study on the elastic modulus of silicone duplex or bi-layer coatings using micro-indentation. Prog Org Coat 2001;41(1–3):135–41.
[4] Jerrams SJ. Friction and adhesion in rigid surface indentation of nitrile rubber. Mater Des 2005, 26(3): 251–258 [special issue Tribology].
[5] Begley MR, Mackin TJ. Spherical indentation of freestanding circular thin films in the membrane regime. J Mech Phys Solids 2004;52(9):2005–23.
[6] Zhang W, Subhash G. Finite element analysis of interacting Vickers indentations on brittle materials. Acta Mater 2001;49(15):2961–74.
[7] Felder E, Bucaille JL. Mechanical analysis of the scratching of metals and polymers with conical indenters at moderate and large strains. Tribol Int 2006;39(2):70–87.
[8] Elleuch R, Elleuch K, Salah B, Zahouani H. Tribological behavior of thermoplastic polyurethane elastomers. Mater Des 2007;28(3):824–30.
[9] Harrison SM, Bush MB, Petros PE. A pinch elastometer for soft tissue. Med Engng Phys 2007;29(3):307–15.
[10] Venu Gopala Rao G, Mahajan P, Bhatnagar N. Micro-mechanical modeling of machining of FRP composites – Cutting force analysis. Compos Sci Technol 2007;67(3–4):579–93.
[11] Rhim SH, Oh SI. Prediction of serrated chip formation in metal cutting process with new flow stress model for AISI 1045 steel. J Mater Process Technol 2006;171(3):417–22.
[12] Mitrofanov AV, Babitsky VI, Silberschmidt VV. Thermomechanical finite element simulations of ultrasonically assisted turning. Comput Mater Sci 2005;32(3–4):463–71.
[13] Zong WJ, Sun T, Li D, Cheng K, Liang YC. FEM optimization of tool geometry based on the machined near surface's residual stresses generated in diamond turning. J Mater Process Technol 2006;180(1–3):271–8.
[14] Zitoune R, Collombet F, Lachaud F, Piquet R, Pasquet P. Experiment–calculation comparison of the cutting conditions representative of the long fiber composite drilling phase. Compos Sci Technol 2005;65(3–4):455–66.
[15] Nagasawa S, Yamagata D, Fukuzawa Y, Murayama M. Stress analysis of wedged rupture in surface layer of coated paperboard. J Mater Process Technol 2006;178(1–3):358–68.
[16] Xie L-J, Schmidt J, Schmidt C, Biesinger F. 2D FEM estimate of tool wear in turning operation. Wear 2005;258(10):1479–90.
[17] Duran A, Nalbant M. Finite element analysis of bending occurring while cutting with high speed steel lathe cutting tools. Mater Des 2005;26(6):549–54.
[18] Ren XJ, Yang QX, James RD, Wang L. Cutting temperatures in hard turning chromium hardfacings with PCBN tooling. J Mater Process Technol 2004;147(1):38–44.
[19] Yen YC, Sohner J, Lilly B, Altan T. Estimation of tool wear in orthogonal cutting using the finite element analysis. J Mater Process Technol 2004;146(1):82–91.
[20] Cakir MC, Isik Y. Finite element analysis of cutting tools prior to fracture in hard turning operations. Mater Des 2005;26(2):105–12.

[21] Gilchrist MD, Keenan S, Curtis M, Cassidy M, Byrne G, Destrade M. Measuring knife stab penetration into skin simulant using a novel biaxial tension device. Forensic Sci Int 2008;177(1):52–65.
[22] Murphy C, Byrne G, Gilchrist MD. The performance of coated WC drills when machining carbon fibre-reinforced epoxy composite materials. J Engng Manuf: IMechE (B) 2002;216:143–52.
[23] McCarthy CT, Hussey M, Gilchrist MD. An investigation into the forces generated when cutting biomaterials with surgical scalpel blades. Key Engng Mater 2005;293–294:769–76.
[24] ABAQUS User Manuals, Version V6.5-1, Dassault Systems; 2007.
[25] BS ISO 37, Rubber, vulcanized or thermoplastic. Determination of tensile stress-strain properties, 3 October, 2005. ISBN:978 0 580 61838.
[26] Ogden RW. Large deformation isotropic elasticity: on the correlation of theory and experiment for incompressible rubberlike solids. Proc Roy Soc 1972;A(326):565–84.
[27] Scott ON, Begley MR, Komaragiri U, Mackin TJ. Indentation of freestanding circular elastomer films using spherical indenters. Acta Mater 2004;52(16):4877–85.
[28] Destrade M, Gilchrist MD, Prikazchikov DA, Saccomandi G. Surface instability of sheared soft tissues. ASME J Biomech Engng 2008;130:061007.
[29] Knight B. The Dynamics of stab wounds. Forensic Sci 1975;6:249–55.
[30] Knight B. In: Forensic pathology. London, Melbourne, Auckland: Edward Arnold; 1991. p. 140–147 p. 212–126.
[31] Ueno Y, Asano M, Nushida H, Adachi J, Tatsuno Y. An unusual case of suicide by stabbing with a falling weighted dagger. Forensic Sci Int 1999;101(3):229–36.
[32] Green MA. Stab wound dynamics: a recording technique for use in medico-legal investigations. J Forensic Sci Soc 1978;18(3–4):161–3.